Environmental Science & Technology

ARTICLE

pubs.acs.org/est

Gaseous Elemental Mercury Capture from Flue Gas Using Magnetic Nanosized $(Fe_{3-x}Mn_x)_{1-\delta}O_4$

Shijian Yang,[†] Naiqiang Yan,[†,*] Yongfu Guo,[†] Daqing Wu,[‡] Hongping He,[‡] Zan Qu,[†] Jianfeng Li,[†] Qin Zhou,[§] and Jingping Jia[†]

[†]School of Environmental Science and Engineering, Shanghai Jiao Tong University, 800 Dong Chuan Road, Shanghai, 200240 P. R. China

[‡]Guangzhou Institute of Geochemistry, Chinese Academy of Sciences, 511 Kehua Street, Wushan, Tianhe District, Guangzhou, 510640 P. R. China

[§]State Key Laboratory of Environmental Aquatic Chemistry, Research Center for Eco-Environmental Sciences, Chinese Academy of Sciences, 18 Shuangqing Road, Haidian District, Beijing, 100085 P. R. China

Supporting Information

ABSTRACT: A series of nanosized $(Fe_{3-x}Mn_x)_{1-\delta}O_4$ (x = 0, 0.2, 0.5, and 0.8) were synthesized for elemental mercury capture from the flue gas. Cation vacancies on $(Fe_{3-x}Mn_x)_{1-\delta}O_4$ can provide the active sites for elemental mercury adsorption, and Mn^{4+} cations on $(Fe_{3-x}Mn_x)_{1-\delta}O_4$ may be the oxidizing agents for elemental mercury oxidization. With the increase of Mn content in the spinel structure, the percents of Mn^{4+} cations and cation vacancies on the surface increased. As a result, elemental mercury capture by $(Fe_{3-x}Mn_x)_{1-\delta}O_4$ was obviously promoted with the increase of Mn content. $(Fe_{2.2}Mn_{0.8})_{1-\delta}O_4$ showed an excellent capacity for elemental mercury capture (>1.5 mg g^{-1} at 100−300 °C) in the presence of SO_2 and HCl. Furthermore, $(Fe_{2.2}Mn_{0.8})_{1-\delta}O_4$ with the saturation magnetization of 45.6 emu g^{-1} can be separated from the fly ash using magnetic separation, leaving the fly ash essentially free of sorbent and adsorbed Hg. Therefore, nanosized $(Fe_{2.2}Mn_{0.8})_{1-\delta}O_4$ may be a promising sorbent for the control of elemental mercury emission.

INTRODUCTION

Mercury is a major pollutant because of its toxicity, mobility, and bioaccumulation in the ecosystem and food chain. The emission of mercury from anthropogenic activities is a serious concern in both the developed and developing countries. Coal-fired utility boilers are currently the largest single-known source of anthropogenic mercury emissions. Mercury exists in three forms in the coal-derived flue gas: elemental mercury (Hg^0), oxidized mercury (Hg^{2+}), and particle-bound mercury (Hg^P).[1] Because elemental mercury is difficult to be removed by currently available pollution control devices, it is the major mercury species emitted in the flue gas.

Many technologies have been investigated to capture elemental mercury from the flue gas. Sorbents/catalysts for elemental mercury capture studied to date mainly fall into one of three groups: carbon-based sorbents, selective catalytic reduction catalysts, and metals and metal oxides.[1] Now, the mercury-sorbent materials are extremely restricted in the application for at least three reasons: sorbent recovery, removal of toxin from the industrial waste, and operation cost.[2−5]

The separation of sorbent from the fly ash can be solved by the magnetic property of sorbent materials.[2−5] A magnetic sorbent MagZ-Ag^0 has been investigated for elemental mercury capture,[6,7] but lower cost sorbents would be more attractive. As is well-known, maghemite (γ-Fe_2O_3) is one of the cheapest magnetic materials. Furthermore, an interesting feature of γ-Fe_2O_3 is the possibility of replacing Fe^{3+} cations by other metal cations while maintaining the spinel structure. Its physicochemical property is strongly dependent on the nature, amount, and site of metal incorporated into the spinel structure. Our previous research demonstrated that Ti^{4+} in γ-Fe_2O_3 can strongly improve its ability for elemental mercury capture, but the presence of a high concentration of SO_2 resulted in a severe interference.[3]

Herein, Mn^{4+} cations were incorporated into γ-Fe_2O_3 to form $(Fe_{3-x}Mn_x)_{1-\delta}O_4$ using a coprecipitation method. Then, $(Fe_{3-x}Mn_x)_{1-\delta}O_4$ was characterized using X-ray diffraction (XRD), H_2 temperature programmed reduction (TPR), N_2 adsorption/desorption isotherm, X-ray photoelectron spectroscopy (XPS), and magnetization measurement. At last, a packed-bed reactor system was used to estimate the performance of $(Fe_{3-x}Mn_x)_{1-\delta}O_4$ for elemental mercury capture.

EXPERIMENTAL SECTION

Samples Preparation. Nanosized $Fe_{3-x}Mn_xO_4$, the precursor of $(Fe_{3-x}Mn_x)_{1-\delta}O_4$, was prepared using a coprecipitation method:[8]

(1) Suitable amounts of ferrous sulfate, ferric chloride, and manganese sulfate were dissolved in distilled water (total cation concentration = 0.30 mol L^{-1}).

(2) The mixture was added to a sodium hydroxide solution (about 1.20 mol L^{-1}), leading to an instantaneous

Received: May 11, 2010
Accepted: December 17, 2010
Revised: December 15, 2010
Published: January 5, 2011

Table 1. Crystal Size, Lattice Parameter, and BET Surface Area of Synthesized $(Fe_{3-x}Mn_x)_{1-\delta}O_4$

$(Fe_{3-x}Mn_x)_{1-\delta}O_4$	crystal size/nm	lattice parameter/nm	BET surface area/$m^2\ g^{-1}$
$x = 0$	12	0.8326	101
$x = 0.2$	14	0.8324	82.9
$x = 0.5$	18	0.8332	69.4
$x = 0.8$	31	0.8346	37.8

precipitation of manganese ferrite according to the following equation

$$2Fe^{3+} + (1\text{-}x)Fe^{2+} + xMn^{2+} + 8OH^- \rightarrow Fe_{3-x}Mn_xO_4 + 4H_2O \quad (1)$$

During the reaction, the system was continuously stirred at 800 rpm.

(3) The particles were then separated by centrifugation at 4500 rpm for 5 min and washed with distilled water followed by a new centrifugation. After 3 washings, the particles were collected and dried in a vacuum oven at 105 °C for 12 h.

γ-Fe_2O_3 was obtained after the thermal treatment of Fe_3O_4 under air at 250 °C for 3 h. $(Fe_{3-x}Mn_x)_{1-\delta}O_4$ (x = 0.2, 0.5, and 0.8) were obtained after the thermal treatment of $Fe_{3-x}Mn_xO_4$ (x = 0.2, 0.5, and 0.8) under air at 400 °C for 3 h. During the oxidization of $Fe_{3-x}Mn_xO_4$ to $(Fe_{3-x}Mn_x)_{1-\delta}O_4$, some cation vacancies (□) were introduced to sustain the spinel structure.

Samples Characterization. Powder XRD pattern was recorded on an X-ray diffractionmeter (Rigaku, D/max-2200/PC) between 10° and 80° at a step of 7° min^{-1} operating at 30 kV and 30 mA using Cu Kα radiation. BET surface area was determined using a nitrogen adsorption apparatus (Micromeritics, ASAP 2010 M+C). The sample was outgassed at 200 °C before BET measurement. TPR profile was recorded on a chemisorption analyzer (Micromeritics, ChemiSorb 2720 TPx) with a gas flow of 20 $cm^3\ min^{-1}$ (10% of hydrogen and 90% of nitrogen) at a rate of 10 °C min^{-1}. Saturation magnetization was determined using a vibrating sample magnetometer (VSM, Model JDM-13) at room temperature. XPS (Thermo, ESCALAB 250) with Al Kα (hv = 1486.6 eV) as the excitation source was used to determine the binding energies of Fe 2p, Mn 2p, S 2p, O 1s, and Hg 4f. The C 1s line at 284.6 eV was taken as a reference for the binding energy calibration.

Elemental Mercury Capture. The assembly used for elemental mercury capture (shown in Figure S1 in the SI) was similar to that described in our previous research.[2−5] A flow of air passed through the permeation tube and yielded a stable concentration of elemental mercury. A temperature control device was employed to keep the reactor at the desired temperatures. The gas containing elemental mercury first passed through the blank tube and then entered the CVAAS to determine the baseline. When the concentration of elemental mercury had fluctuated within ±5% for more than 30 min, the gas was diverted to pass through the adsorbent bed. An exact amount of sorbent was inserted in the middle of the column reactor and then packed with quartz wool to support the sorbent layer and to avoid its loss. It was demonstrated that quartz wool has no ability for elemental mercury capture.

To preliminarily estimate the performance for elemental mercury capture, $(Fe_{3-x}Mn_x)_{1-\delta}O_4$ was first tested under air. The inlet gas contained a stable concentration of elemental mercury (shown in Table S1 in the SI) with a feed of 12 L h^{-1}. The test time for $(Fe_{3-x}Mn_x)_{1-\delta}O_4$ ($x \neq 0$) was about 10 h. Because the breakthrough ratios of γ-Fe_2O_3 for elemental mercury capture were more than 90% within 4 h, the test time for γ-Fe_2O_3 was about 4 h. For each test, the sorbent mass was about 25.0 mg (the gas space velocity was about $1.2 \times 10^6\ h^{-1}$), and the reaction temperature varied from 100 to 300 °C.

The effect of a high concentration of SO_2 on elemental mercury capture was investigated. The inlet gas contained about 2.8 g Nm^{-3} (1000 ppmv) of SO_2 and 10% of O_2. Furthermore, the effect of HCl on elemental mercury capture was investigated. The inlet gas contained about 2.8 g Nm^{-3} of SO_2, 8.1 mg Nm^{-3} (5 ppmv) of HCl, and 10% of O_2.

The concentration of elemental mercury in the gas was analyzed using a SG-921 CVAAS. Meanwhile, Hg^{2+} in the gas at the exit of reactor was absorbed by 1.0 mol L^{-1} of KCl. Then, the amount of Hg^{2+} in the KCl solution was determined using the CVAAS. Breakthrough curve was generated by plotting the concentration of elemental mercury in the gas at the exit of reactor.

RESULTS AND DISCUSSION

Characterization. The characteristic reflections of synthesized samples (shown in Figure S2 in the SI) corresponded very well to the standard card of maghemite (JCPDS: 39-1346). Additional reflections that would indicate the presence of other crystalline manganese oxides, such as Mn_3O_4, Mn_2O_3, or MnO_2, were not present in the diffraction scan. Furthermore, the lattice parameter of synthesized $Fe_{2.2}Mn_{0.8}O_4$ was 0.8456 nm (XRD pattern is not shown), which was much larger than that of magnetite (0.8396 nm). These indicate that Mn cations were incorporated into the spinel structure. Crystal sizes of synthetic samples were calculated with the Scherrer's equation.[9] As shown in Table 1, the crystal size increased with the increase of Mn content in $(Fe_{3-x}Mn_x)_{1-\delta}O_4$.

TPR profile of γ-Fe_2O_3 showed two obvious reduction peaks (shown in Figure 1A). The peak centered at about 370 °C corresponded to the reduction of γ-Fe_2O_3 to Fe_3O_4, and the broad peak at the higher temperature was attributed to the reduction of Fe_3O_4 to Fe^0.[10] TPR profiles of $(Fe_{3-x}Mn_x)_{1-\delta}O_4$ ($x \neq 0$) showed three groups of reduction peaks (shown in Figure 1A). The peaks centered at about 345−362 °C corresponded to the reduction of $(Fe_{3-x}Mn_x)_{1-\delta}O_4$ to $Fe_{3-x}Mn_xO_4$, the peaks centered at about 520−598 °C were attributed to the reduction of $Fe_{3-x}Mn_xO_4$ to manganowustite ($Fe_{1-y}Mn_yO$), and the last peaks were assigned to the reduction of $Fe_{1-y}Mn_yO$ to Fe^0 and MnO.[11] As Mn was introduced into the spinel structure, the first peak shifted to a lower temperature. Meanwhile, the area of the first peak decreased with the increase of Mn content in $(Fe_{3-x}Mn_x)_{1-\delta}O_4$. It may be related to the decrease of the BET surface area (shown in Table 1). The reduction of $(Fe_{3-x}Mn_x)_{1-\delta}O_4$ to $Fe_{3-x}Mn_xO_4$ involved the reduction of Mn^{4+} to Mn^{3+}, Mn^{3+} to Mn^{2+}, and partial Fe^{3+} to Fe^{2+}. As shown in Figure 1B, the H_2 consumption at <300 °C corresponding to the reduction of Mn^{4+} cations on the surface obviously increased with the increase of Mn content in $(Fe_{3-x}Mn_x)_{1-\delta}O_4$. It indicates that the amount of Mn^{4+} cations on $(Fe_{3-x}Mn_x)_{1-\delta}O_4$ increased with the increase of Mn content.

A key feature of the novel sorbent is its magnetic property, which makes it possible to separate the sorbent from the fly ash mixture. The saturation magnetizations of $(Fe_{3-x}Mn_x)_{1-\delta}O_4$ (x = 0, 0.2, 0.5, and 0.8) were 59.0, 48.6, 45.4, and 45.6 emu g^{-1},

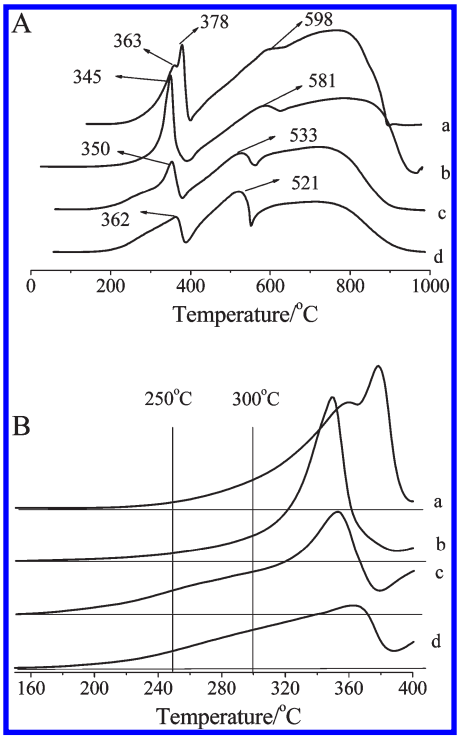

Figure 1. (A) TPR profiles of synthesized $(Fe_{3-x}Mn_x)_{1-\delta}O_4$ and (B) expansion of TPR profiles of synthesized $(Fe_{3-x}Mn_x)_{1-\delta}O_4$ from 150 to 400 °C: (a), $x = 0$; (b), $x = 0.2$; (c), $x = 0.5$; (d), $x = 0.8$.

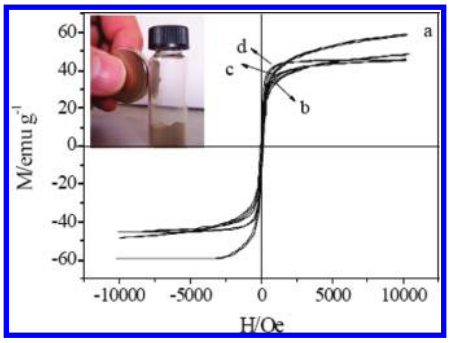

Figure 2. Magnetization characteristics of synthesized $(Fe_{3-x}Mn_x)_{1-\delta}O_4$: (a) $x = 0$; (b) $x = 0.2$; (c) $x = 0.5$; (d) $x = 0.8$.

respectively. $(Fe_{3-x}Mn_x)_{1-\delta}O_4$ showed the superparamagnetism with a minimized coercivity and a negligible magnetization hysteresis (shown in Figure 2). The magnetization characteristic ensures that the magnetic sorbents cannot be permanently magnetized after being exposed to an external magnetic field. Therefore, the sorbent particles can be redispersed without aggregation when the magnetic field is removed.[6]

The peaks of Fe species on $(Fe_{2.2}Mn_{0.8})_{1-\delta}O_4$ were assigned to oxidized Fe species, more likely Fe^{3+} type species. The binding energies centered at about 709.9 and 711.1 eV may be assigned to Fe^{3+}cations in the spinel structure, and the binding energy centered at about 712.3 eV may be ascribed to Fe^{III}−OH (shown in Figure 3a). The Mn peaks at 641.1 and 642.4 eV were assigned to Mn^{3+} and Mn^{4+}, respectively (shown in Figure 3b). As shown in Table 2, the percent of Mn^{4+} on $(Fe_{3-x}Mn_x)_{1-\delta}O_4$ obviously increased with the increase of Mn content. The O peak mainly centered at about 529.9 eV (shown in Figure 3c), as expected for the transition metal oxides. Another oxygen species at about 531.3 eV was also observed, which was assigned to −OH.

Elemental Mercury Capture under Air. The determination of oxidized mercury concentration at the exit of reactor showed that there was little oxidized mercury in the gas after passing through the reactor tube with $(Fe_{3-x}Mn_x)_{1-\delta}O_4$. It indicates that the reduced amount of elemental mercury in the breakthrough curve (shown in Figure S3a-c in the SI) was captured by the magnetic sorbent. The mass of elemental mercury captured per unit mass of sorbent (capacity) can be calculated from the breakthrough curve. As shown in Table 3, the capacity of $(Fe_{3-x}Mn_x)_{1-\delta}O_4$ for elemental mercury capture generally increased with the increase of Mn content. With the continuous increase of reaction temperature from 100 to 300 °C, the capacities of $(Fe_{3-x}Mn_x)_{1-\delta}O_4$ for elemental mercury capture showed the same variation tendency, and the optimal reaction temperatures all centered at about 250 °C.

Elemental mercury capture by metal oxides in the absence of halogen is generally attributed to the Mars-Maessen mechanism.[1,12] The mechanism for elemental mercury capture by $(Fe_{3-x}Mn_x)_{1-\delta}O_4$ was studied using XPS analysis. In comparison with fresh $(Fe_{2.2}Mn_{0.8})_{1-\delta}O_4$ (shown in Figure 3a-c), no obvious changes happened in the XPS spectra over the spectral regions of Fe 2p and O 1s (shown in Figure 3d and e). As shown in Figure 3f, the component centered at about 640.4 eV corresponding to Mn^{2+} cations did not appear. Meanwhile, the ratio of Mn^{4+} cation to Mn^{3+} cation decreased from 1.57 to 1.37 after elemental mercury capture. They suggest that some Mn^{4+} cations were reduced to Mn^{3+} cations during elemental mercury capture. Taking account of the binding energy of Hg 4f7/2 at 100.1 eV and the absence of Hg 4f 5/2 at about 105 eV corresponding to Hg^{2+} (shown in Figure 3g), the oxidized mercury formed may be mercurous oxide. Mercurous oxide has been previously observed on $(Fe_2Ti)_{0.8}O_4$ and $(Fe_2Ti_{0.8}Mn_{0.2})_{1-\delta}O_4$ in our previous research.[3,4] Therefore, the mechanism of elemental mercury capture by $(Fe_{3-x}Mn_x)_{1-\delta}O_4$ can be described as

$$Hg^0_{(g)} + \equiv\square \rightarrow \equiv\square - Hg^0_{(ad)} \quad (2)$$

$$\equiv\square - Hg^0 + \equiv Mn^{IV} \rightarrow \equiv Mn^{III}Hg^I \quad (3)$$

Reaction 2 was the collision of elemental mercury with the surface, resulting in a physical adsorption on the cation vacancies. Cation vacancies on the surface are typical Lewis acid sites.[2−5] Gaseous elemental mercury is a Lewis base because it can be an electron-pair donor. The term Lewis base is more general and refers to the propensity to complex with a Lewis acid. If the concentration of elemental mercury in gas phase was sufficiently high for the surface to be saturated with physically adsorbed elemental mercury, the concentration of physically adsorbed elemental mercury on the surface ($[\equiv\square\text{-}Hg^0]$) can be described as

$$[\equiv\square - Hg^0] = k_1[\equiv\square] \quad (4)$$

where $[\equiv\square]$ and k_1 were the percent of cation vacancies on the surface and the constant, respectively. Reaction 2 was an exothermic reaction, so k_1 would rapidly decrease with the increase of reaction temperature.

Reaction 3 was the oxidation of physically adsorbed elemental mercury to a Mn−Hg bimetal oxide by Mn^{4+} cations on the surface.[12]

As is well-known, mercury is a heavy metal, and its atomic radius (1.76 Å) is much bigger than the radiuses of Mn^{4+} (0.60 Å), Mn^{3+} (0.66 Å), Fe^{3+} (0.64 Å), and O^{2-} (1.32 Å). When a mercury atom is

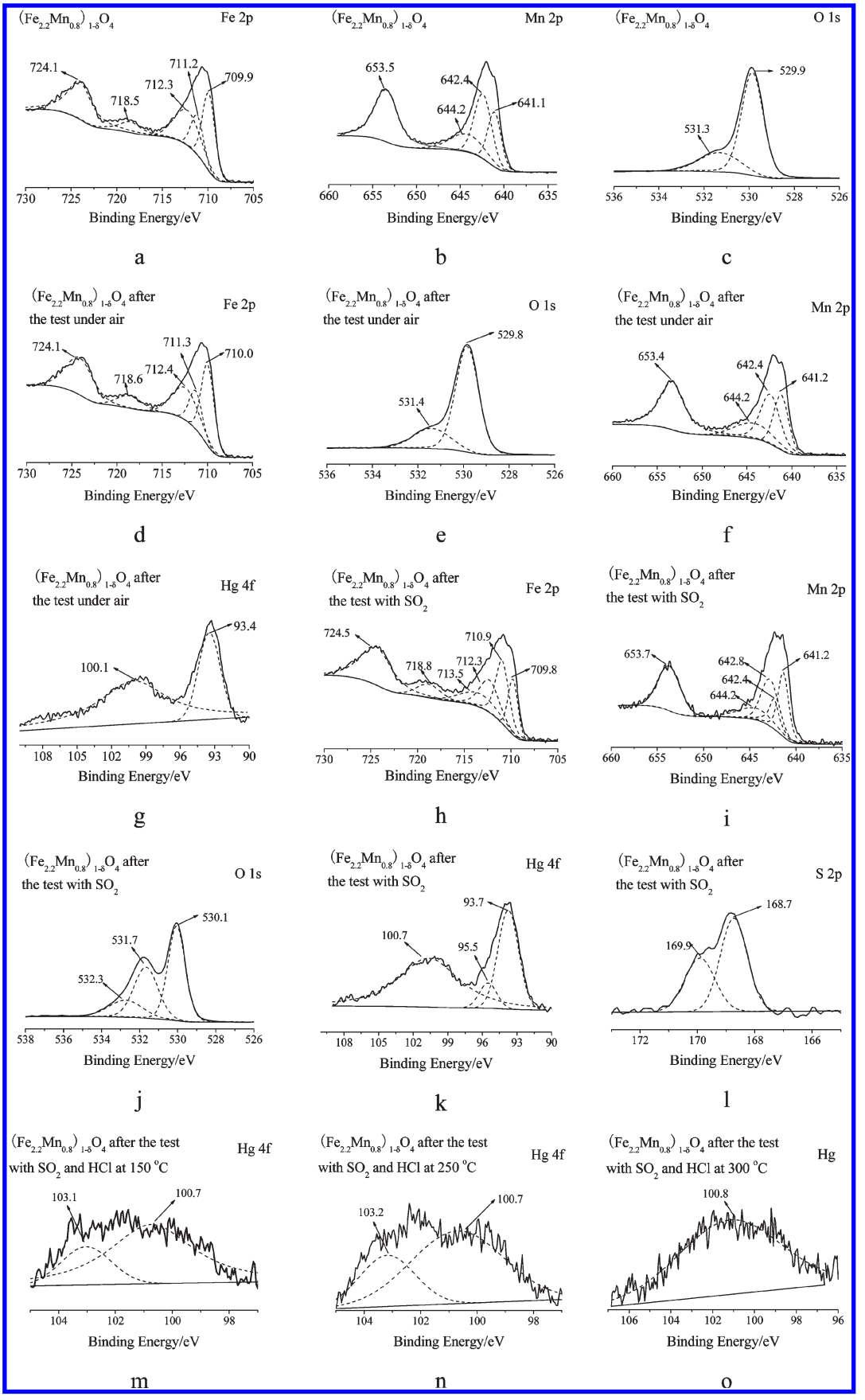

Figure 3. XPS spectra of $(Fe_{2.2}Mn_{0.8})_{1-\delta}O_4$ over the spectral regions of Fe 2p, Mn 2p, O 1s, Hg 4f, and S 2p.

dx.doi.org/10.1021/es103391w |*Environ. Sci. Technol.* 2011, 45, 1540–1546

Table 2. Data of Atomic Ratios on the Surface Collected from XPS Analysis/%

$(Fe_{3-x}Mn_x)_{1-\delta}O_4$	□	Mn	Mn^{2+}	Mn^{3+}	Mn^{4+}	BET[≡□] $[\equiv Mn^{IV}]_0/m^2\ g^{-1}$
$x = 0.2$	4.7	5.1	1.9	1.6	1.6	0.062
$x = 0.5$	6.4	13.6	-	7.6	6.0	0.27
$x = 0.8$	8.1	18.5	-	7.2	11.3	0.35

physically adsorbed on the cation vacancy, several ions including Mn^{4+}, Mn^{3+}, Fe^{3+}, and O^{2-} around the cation vacancy may be covered. Once the adsorbed elemental mercury contacts Mn^{4+} cation on the surface, the adsorbed elemental mercury will be oxidized.

The array of cation vacancies, Mn^{3+}/Mn^{4+}, Fe^{3+}, and O^{2-} in/on $(Fe_{3-x}Mn_x)_{1-\delta}O_4$ was well-proportioned even at the atomic scale due to the incorporation of Mn cations into the spinel structure. The near two Mn cations on $(Fe_{3-x}Mn_x)_{1-\delta}O_4$ were spaced at least by two Fe cations and four oxygen anions, so the distance between two Mn^{4+} cations was much more than the diameter of the Hg atom. When a mercury atom was physically adsorbed on the active site (i.e., □), at most one Mn^{4+} cation can be covered. Therefore, reaction 3 happened. As is well-known, Hg_2O is not stable and it can self-decompose to HgO and Hg at a high temperature. Because the oxidized mercury formed on $(Fe_{3-x}Mn_x)_{1-\delta}O_4$ was isolated $Mn^{III}Hg^{I}O_2$, the near two oxidized mercury formed were spaced at least by two Fe cations and four oxygen anions. As a result, two mercurous cations cannot collide to transform to one Hg atom and one Hg^{2+} cation. Therefore, the formed mercurous oxide on $(Fe_{3-x}Mn_x)_{1-\delta}O_4$ was stable (shown in Figure S3).

The kinetic equation of reaction 3 can be described as

$$-\frac{d[\equiv Mn^{IV}]}{dt} = -\frac{d[\equiv\square - Hg^0]}{dt} = \frac{d[\equiv Mn^{III}Hg^{I}]}{dt} = k[\equiv Mn^{IV}][\equiv\square - Hg^0] \quad (5)$$

where $[\equiv Mn^{IV}]$, $[\equiv Mn^{III}Hg^{I}]$, and k were the percent of Mn^{4+} cation, the percent of the bimetal oxide on the surface, and the kinetic constant, respectively. Because reaction 3 was promoted with the increase of reaction temperature, k would increase with the increase of reaction temperature.

According to eq 5, $[\equiv Mn^{IV}]$ may be approximately described as

$$[\equiv Mn^{IV}] = [\equiv Mn^{IV}]_0 \exp(-k[\equiv\square - Hg^0]t) = [\equiv Mn^{IV}]_0 \exp(-kk_1[\equiv\square]t) \quad (6)$$

Then,

$$\frac{d[\equiv Mn^{III}Hg^{I}]}{dt} = kk_1[\equiv\square][\equiv Mn^{IV}]_0 \exp(-kk_1[\equiv\square]t) \quad (7)$$

$$[\equiv Mn^{III}Hg^{I}] = kk_1[\equiv\square][\equiv Mn^{IV}]_0 \int_0^t \exp(-kk_1[\equiv\square]t)dt \quad (8)$$

So,

$$Q = BETkk_1[\equiv\square][\equiv Mn^{IV}]_0 \int_0^t \exp(-kk_1[\equiv\square]t)dt \quad (9)$$

Table 3. Capacity of $(Fe_{3-x}Mn_x)_{1-\delta}O_4$ for Elemental Mercury Capture mg g^{-1}

$(Fe_{3-x}Mn_x)_{1-\delta}O_4$	100 °C	150 °C	200 °C	250 °C	300 °C
$x = 0$	<0.20	<0.20	0.26	0.44	0.34
$x = 0.2$	1.92	1.80	1.60	2.20	0.84
$x = 0.5$	2.90	2.92	2.42	4.26	1.74
$x = 0.8$	2.86	3.20	4.44	5.10	1.04
$x = 0.8$ with SO_2	2.38	1.92	1.72	2.48	0.96
$x = 0.8$ with SO_2 and HCl	2.01	1.92	2.07	1.54	2.21

where Q was the amount of elemental mercury captured, which can be described as the product of $[\equiv Mn^{III}Hg^{I}]$ and BET surface area. As shown in eq 9, Q should be approximately proportional to the product of BET, $[\equiv\square]$, and $[\equiv Mn^{IV}]_0$. There generally was a positive correlation between $BET[\equiv\square][\equiv Mn^{IV}]_0$ and the capacity of $(Fe_{3-x}Mn_x)_{1-\delta}O_4$ for elemental mercury capture (shown in Tables 2 and 3), so the increase of Mn^{4+} cations and cation vacancies on the surface may mainly account for the prominent promotion of elemental mercury capture by $(Fe_{3-x}Mn_x)_{1-\delta}O_4$ due to the increase of Mn content.

Although reaction 3 was promoted with the increase of reaction temperature, elemental mercury capture reached the optimal condition at a specific temperature, in most cases not the highest temperature due to the influence of reaction temperature on the physical adsorption (reaction 2). Mn^{4+} cation on $(Fe_{2.2}Mn_{0.8})_{1-\delta}O_4$ may be easier to be reduced by □ to form Mn^{3+} cation at higher temperatures,[13] so the capacity of $(Fe_{2.2}Mn_{0.8})_{1-\delta}O_4$ for elemental mercury capture at 300 °C was much less than that of $(Fe_{2.5}Mn_{0.5})_{1-\delta}O_4$.

Effect of SO_2 on Elemental Mercury Capture by $(Fe_{2.2}Mn_{0.8})_{1-\delta}O_4$. The chemical composition in the flue gas significantly affects elemental mercury capture by sorbents. The components in the real coal-fired flue gas which can interfere with elemental mercury capture are mainly a high concentration of SO_2/SO_3.[14,15] SO_2 gas molecules may compete with gaseous elemental mercury for the active sites. The concentration of SO_2 in the real flue gas is about 10^4-10^5 times that of elemental mercury (v/v).[14]

The determination of oxidized mercury concentration at the exit of reactor showed that there was little oxidized mercury in the gas after passing through the reactor tube with $(Fe_{2.2}Mn_{0.8})_{1-\delta}O_4$ in the presence of 1000 ppmv of SO_2. It indicates that the reduced amount of elemental mercury in the breakthrough curve (shown in Figure S3d in the SI) was captured by $(Fe_{2.2}Mn_{0.8})_{1-\delta}O_4$. Table 3 shows that the presence of a high concentration of SO_2 resulted in an obvious interference with elemental mercury capture by $(Fe_{2.2}Mn_{0.8})_{1-\delta}O_4$. However, $(Fe_{2.2}Mn_{0.8})_{1-\delta}O_4$ still showed an excellent capacity for elemental mercury capture (>1.70 mg g^{-1} at 100−250 °C) in the presence of 1000 ppmv of SO_2.

Previous research postulated a mechanism for the heterogeneous uptake and oxidization of SO_2 on iron oxides,[16] and the reactions can be described as

$$\equiv Fe^{III} - OH + SO_{2(g)} \rightarrow \equiv Fe^{III}OSO_2^- + H^+ \quad (10)$$

$$\equiv Fe^{III}OSO_2^- \rightarrow \equiv Fe^{II} + SO_3^{*-} \quad (11)$$

$$\equiv Fe^{III} - OH + SO_3^{*-} \rightarrow \equiv Fe^{II} + HSO_4^- \quad (12)$$

As shown in reactions 10-12, the uptake of SO_2 on iron oxides may involve hydroxyl groups on the surface. Furthermore, SO_2 can also react with Mn^{4+} cations on the surface,[17] and the reaction can be described as

$$SO_{2(g)} + \equiv Mn^{IV} + 2 \equiv O \rightarrow \equiv Mn^{II} + SO_4^{2-} \quad (13)$$

If reaction 13 happened, elemental mercury capture by $(Fe_{2.2}Mn_{0.8})_{1-\delta}O_4$ would be interfered.

Elemental mercury capture by $(Fe_{2.2}Mn_{0.8})_{1-\delta}O_4$ in the presence of a high concentration of SO_2 at 150 °C was also studied using XPS (shown in Figure 3h-l). The S peaks mainly centered at 168.7 and 169.9 eV, which may be assigned to SO_4^{2-} and HSO_4^-, respectively. The formation of SO_4^{2-} can also be supported by the spectra of Fe 2p, Mn 2p, and O 1s. Three new peaks appeared in the spectra of Fe 2p (713.5 eV), Mn 2p (642.8 eV), and O 1s (532.3 eV), which may be assigned to Fe^{3+} in $Fe_2(SO_4)_3$, Mn^{2+} in $MnSO_4$, and O^{2-} in SO_4^{2-}, respectively. XPS analysis showed that 39% of Mn cations on $(Fe_{2.2}Mn_{0.8})_{1-\delta}O_4$ transformed to $MnSO_4$. It demonstrates that SO_2 reacted with Mn^{4+} on $(Fe_{2.2}Mn_{0.8})_{1-\delta}O_4$ to form a surface sulfate species and then interfered with elemental mercury capture. XPS analysis also showed that 65% of the transformation of SO_2 to SO_4^{2-} involved Fe cations on the surface, and only 35% involved Mn cations on the surface. As a result, the high concentration of SO_2 showed a moderate effect on elemental mercury capture by $(Fe_{2.2}Mn_{0.8})_{1-\delta}O_4$, which was much less than it on elemental mercury capture by $(Fe_2Ti)_{0.8}O_4$.[3] Taking into account the binding energy of Hg 4f7/2 at 100.7 eV and the absence of Hg 4f 5/2 at about 105 eV corresponding to Hg^{2+} (shown in Figure 3k), the oxidized mercury formed in the presence of SO_2 may be mercurous sulfate. Mercurous sulfate has been previously observed during the photochemical removal of elemental mercury from the flue gas.[18,19] Our previous research also demonstrated that mercurous sulfate formed during elemental mercury capture by $(Fe_2Ti)_{0.8}O_4$ and $(Fe_2Ti_{0.8}Mn_{0.2})_{1-\delta}O_4$ in the presence of a high concentration of SO_2.[3,4]

Effect of HCl on Elemental Mercury Capture by $(Fe_{2.2}Mn_{0.8})_{1-\delta}O_4$. The presence of HCl in the flue gas may enhance elemental mercury oxidization, and the formed $HgCl_2$ may sublime into the flow at 300 °C.[20] So the effect of HCl on elemental mercury capture by $(Fe_{2.2}Mn_{0.8})_{1-\delta}O_4$ was investigated.

The determination of oxidized mercury concentration at the exit of reactor still showed that there was little oxidized mercury in the gas after passing through the reactor tube with $(Fe_{2.2}Mn_{0.8})_{1-\delta}O_4$ in the presence of 1000 ppmv of SO_2 and 5 ppmv of HCl. It indicates that the reduced amount of elemental mercury in the breakthrough curve (shown in Figure S3e in the SI) was captured by $(Fe_{2.2}Mn_{0.8})_{1-\delta}O_4$. As shown in Table 3, the presence of HCl resulted in an insignificant effect on elemental mercury capture at 100−200 °C. But it showed a moderate interference and an obvious promotion at 250 and 300 °C, respectively.

Taking account of the binding energy of Hg4f7/2 at about 100.7 eV and the absence of Hg 4f 5/2 at about 105 eV corresponding to Hg^{2+}, the oxidized mercury formed in the presence of SO_2 and HCl may still be mercurous sulfate or HgCl (shown in Figure 3m-o). The binding energy centered at about 103.2 eV was attributed to Si 2p of SiO_2 in quartz wool.

The possible routes of HCl uptake on $(Fe_{2.2}Mn_{0.8})_{1-\delta}O_4$ can be described as

$$\equiv Fe^{III}\text{-}OH + HCl_{(g)} \rightarrow \equiv Fe^{III} + Cl^- + H_2O \quad (14)$$

$$\equiv Mn^{4+} + HCl_{(g)} \rightarrow \equiv Mn^{III} + Cl^*_{(ad)} + H^+ \quad (15)$$

Reaction 14 may predominate over the uptake of HCl on $(Fe_{2.2}Mn_{0.8})_{1-\delta}O_4$ at 100−200 °C, so the presence of 5 ppmv of HCl showed an insignificant effect on elemental mercury capture by $(Fe_{2.2}Mn_{0.8})_{1-\delta}O_4$. The amount of $\equiv Fe^{III}-OH$ would decrease with the increase of reaction temperature due to the dehydration, so reaction 15 may predominate over the uptake of HCl on $(Fe_{2.2}Mn_{0.8})_{1-\delta}O_4$ at 250−300 °C. There may be a large number of SO_2 adsorbed on $(Fe_{2.2}Mn_{0.8})_{1-\delta}O_4$ at 250 °C, so the formed $Cl_{(ad)}$* may be eliminated by the adsorbed SO_2. As a result, the presence of 5 ppmv of HCl showed a moderate interference with elemental mercury capture at 250 °C. Furthermore, the oxidized mercury formed may still be mercurous sulfate at 100−200 °C. Most of SO_2 would desorb from $(Fe_{2.2}Mn_{0.8})_{1-\delta}O_4$ with the further increase of reaction temperature, so the Langmuir−Hinshelwood mechanism may mainly account for the oxidization of elemental mercury at 300 °C. The near two Mn^{4+} cations on $(Fe_{2.2}Mn_{0.8})_{1-\delta}O_4$ were spaced at least by two Fe cations and four oxygen anions, so the formed $Cl^*_{(ad)}$ may also be spaced by two Fe cations and four oxygen anions. When a mercury atom was physically adsorbed on the active site (i.e., □), at most one $Cl^*_{(ad)}$ can be covered, so reaction 16 happened and the oxidized mercury formed was HgCl

$$\equiv\square - Hg + Cl^*_{(ad)} \rightarrow Hg^ICl_{(ad)} \quad (16)$$

The kinetic constant of reaction 16 may be much more than that of reaction 3, so elemental mercury capture by $(Fe_{2.2}Mn_{0.8})_{1-\delta}O_4$ at 300 °C was promoted by 5 ppmv of HCl. As well-known, Hg_2Cl_2 is not stable, and it can self-decompose to $HgCl_2$ and Hg at a high temperature. Because HgCl formed on $(Fe_{2.2}Mn_{0.8})_{1-\delta}O_4$ was spaced at least by two Fe cations and four oxygen anions, the near two HgCl cannot collide to transform to one Hg and one $HgCl_2$. As a result, the formed HgCl was stable and Hg^{2+} was undetected at the exit of the reactor.

Magnetic Separation. Although the crystal sizes of synthesized $(Fe_{3-x}Mn_x)_{1-\delta}O_4$ were less than 50 nm, their particulate sizes were higher than 100 μm due to the agglomeration after the thermal treatment. The magnetic sorbent can be recovered in situ by a two-step process. The magnetic sorbent can first be removed from the flue gas as a mixture with the fly ash particles by an electrostatic precipitator or fabric filter, followed by the magnetic separation of the sorbent and adsorbed mercury from the fly ash. Previous research demonstrated that the magnetic sorbent MagZ-Ag^0 with the saturation magnetization of 40 emu g^{-1} and the BET surface area of 164 m^2 g^{-1} can be easily separated from the fly ash.[6,7] The photograph inserted in Figure 2 shows the result of separating $(Fe_{2.2}Mn_{0.8})_{1-\delta}O_4$ from the mixture with 10 g of fly ash and 1 g of $(Fe_{2.2}Mn_{0.8})_{1-\delta}O_4$ by a normal magnet. After $(Fe_{2.2}Mn_{0.8})_{1-\delta}O_4$ was separated from the mixture, the contents of Mn and Fe in the fly ash did not increase. It indicates that $(Fe_{2.2}Mn_{0.8})_{1-\delta}O_4$ can be separated from the fly ash using magnetic separation, leaving the fly ash essentially free of sorbent and adsorbed mercury. Magnetic separation has been widely used in the mineral processing,[21] and the device of the equipment for the magnetic separation of the sorbent from the fly ash may be modeled on that used in the mineral processing.

In summary, $(Fe_{2.2}Mn_{0.8})_{1-\delta}O_4$ showed an excellent capacity for elemental mercury capture. Meanwhile, its inherent magnetization made it possible to separate $(Fe_{2.2}Mn_{0.8})_{1-\delta}O_4$ from the fly ash, leaving the fly ash essentially free of sorbent and adsorbed mercury. Therefore, $(Fe_{2.2}Mn_{0.8})_{1-\delta}O_4$ may be a promising sorbent for the control of elemental mercury emission. In our future work, $(Fe_{2.2}Mn_{0.8})_{1-\delta}O_4$ will be investigated to capture elemental mercury from the flue gas at a pilot scale, in which the separation of sorbent from the fly ash and sorbent regeneration will be further studied.

■ ASSOCIATED CONTENT

Supporting Information. Text, Figures S1-S3, and Tables S1 and S2. This material is available free of charge via the Internet at http://pubs.acs.org.

■ AUTHOR INFORMATION

Corresponding Author
*Phone: 86-21-54745591; e-mail: nqyan@sjtu.edu.cn.

■ ACKNOWLEDGMENT

This study was supported by the High-Tech R&D Program of China (No. 2007AA06Z340) and Shanghai Tongji Gao Tingyao Environmental Science & Technology Development Foundation.

■ REFERENCES

(1) Presto, A. A.; Granite, E. J. Survey of catalysts for oxidation of mercury in flue gas. *Environ. Sci. Technol.* **2006**, *40*, 5601–5609.

(2) Yang, S. J.; Guo, Y. F.; Yan, N. Q.; Qu, Z.; Xie, J. K.; Yang, C.; Jia, J. P. Capture of gaseous elemental mercury from flue gas using a magnetic and sulfur poisoning resistant sorbent Mn/γ-Fe_2O_3 at lower temperatures. *J. Hazard. Mater.* **2010**, doi:10.1016/j.jhazmat.2010.11.034.

(3) Yang, S. J.; Guo, Y. F.; Yan, N. Q.; Wu, D. Q.; He, H. P.; Qu, Z.; Yang, C.; Zhou, Q.; Jia, J. P. Nanosized cation-deficient Fe-Ti Spinel: A novel magnetic sorbent for elemental mercury capture from flue gas. *ACS Appl. Mater. Inter.* **2010**, under revision.

(4) Yang, S. J.; Guo, Y. F.; Yan, N. Q.; Wu, D. Q.; He, H. P.; Xie, J. K.; Qu, Z.; Jia, J. P. Remarkable effect of the incorporation of titanium on the catalytic activity and SO_2 poisoning resistance of magnetic Mn-Fe spinel for elemental mercury capture. *Appl. Catal., B* **2010**, *101*, 698−708.

(5) Yang, S. J.; Guo, Y. F.; Yan, N. Q.; Wu, D. Q.; He, H. P.; Xie, J. K.; Qu, Z.; Yang, C.; Jia, J. P. A novel muti-functional magnetic Fe-Ti-V spinel catalyst for elemental mercury capture and callback from flue gas. *Chem. Commun.* **2010**, *46*, 8377–8379.

(6) Dong, J.; Xu, Z. H.; Kuznicki, S. M. Magnetic multi-functional nano composites for environmental applications. *Adv. Funct. Mater.* **2009**, *19*, 1268–1275.

(7) Dong, J.; Xu, Z. H.; Kuznicki, S. M. Mercury removal from flue gases by novel regenerable magnetic nanocomposite sorbents. *Environ. Sci. Technol.* **2009**, *43*, 3266–3271.

(8) Kodama, T.; Ookubo, M.; Miura, S.; Kitayama, Y. Synthesis and characterization of ultrafine Mn(II)-bearing ferrite of type $Mn_xFe_{3-x}O_4$ by coprecipitation. *Mater. Res. Bull.* **1996**, *31*, 1501–1512.

(9) Yang, S. J.; He, H. P.; Wu, D. Q.; Chen, D.; Liang, X. L.; Qin, Z. H.; Fan, M. D.; Zhu, J. X.; Yuan, P. Decolorization of methylene blue by heterogeneous Fenton reaction using $Fe_{3-x}Ti_xO_4$ ($0 \le x \le 0.78$) at neutral pH values. *Appl. Catal., B* **2009**, *89*, 527–535.

(10) Ayub, I.; Berry, F. J.; Crabb, E.; Helgason, O. Titanium-doped γ-Fe_2O_3: Reduction and oxidation properties. *J. Mater. Sci.* **2004**, *39*, 6921–6927.

(11) Oliveira, L. C. A.; Fabris, J. D.; Rios, R.; Mussel, W. N.; Lago, R. M. $Fe_{3-x}Mn_xO_4$ catalysts: phase transformations and carbon monoxide oxidation. *Appl. Catal., A* **2004**, *259*, 253–259.

(12) Granite, E. J.; Pennline, H. W.; Hargis, R. A. Novel sorbents for mercury removal from flue gas. *Ind. Eng. Chem. Res.* **2000**, *39*, 1020–1029.

(13) Gillot, B.; Laarj, M.; Kacim, S. Reactivity towards oxygen and cation distribution of manganese iron spinel $Mn_{3-x}Fe_xO_4$ ($0 \le x \le 3$) fine powders studied by thermogravimetry and IR spectroscopy. *J. Mater. Chem.* **1997**, *7*, 827–831.

(14) Presto, A. A.; Granite, E. J. Impact of sulfur oxides on mercury capture by activated carbon. *Environ. Sci. Technol.* **2007**, *41*, 6579–6584.

(15) Presto, A. A.; Granite, E. J.; Karash, A. Further investigation of the impact of sulfur oxides on mercury capture by activated carbon. *Ind. Eng. Chem. Res.* **2007**, *46*, 8273–8276.

(16) Fu, H. B.; Wang, X.; Wu, H. B.; Yin, Y.; Chen, J. M. Heterogeneous uptake and oxidation of SO_2 on iron oxides. *J. Phys. Chem. C* **2007**, *111*, 6077–6085.

(17) Yu, J.; Guo, F.; Wang, Y. L.; Zhu, J. H.; Liu, Y. Y.; Su, F. B.; Gao, S. Q.; Xu, G. W. Sulfur poisoning resistant mesoporous Mn-base catalyst for low-temperature SCR of NO with NH_3. *Appl. Catal., B* **2010**, *95*, 160–168.

(18) McLarnon, C. R.; Granite, E. J.; Pennline, H. W. The PCO process for photochemical removal of mercury from flue gas. *Fuel Process. Technol.* **2005**, *87*, 85–89.

(19) Granite, E. J.; Pennline, H. W.; Hoffman, J. S. Effects of photochemical formation of mercuric oxide. *Ind. Eng. Chem. Res.* **1999**, *38*, 5034–5037.

(20) Schofield, K. Fuel-mercury combustion emissions: An important heterogeneous mechanism and an overall review of its implications. *Environ. Sci. Technol.* **2008**, *42*, 9014–9030.

(21) Shen, H. T.; Forssberg, E. An overview of recovery of metals from slags. *Waste Manage.* **2003**, *23*, 933–949.